Free-space competition between gain-swept superradiance and spontaneous emission from N₂⁺ in a femtosecond filament

Yuxuan Zhang [1,*], Yitan Gao [2,3,*], Hongbin Lei [4,*], Zoumingyang Zhu [1], Bitao Hu,[1] Kun Zhao [2,3], Zengxiu Zhao [4], Pengji Ding [1,†], and Zuoye Liu[1,‡]

[1]*Frontiers Science Center for Rare Isotopes and School of Nuclear Science and Technology, Lanzhou University, 730000 Lanzhou, China*
[2]*Songshan Lake Materials Laboratory, Dongguan 523808, China*
[3]*Beijing National Laboratory for Condensed Matter Physics, Institute of Physics, Chinese Academy of Sciences, Beijing 100190, China*
[4]*Department of Physics, National University of Defense Technology, Changsha 410073, China*

Air lasing from the singly ionized nitrogen molecule N₂⁺ in a femtosecond laser filament under low gas pressures has been of intense interest in the field of ultrafast optics in the past decade. Several theoretical models have been proposed to explain the origin of N₂⁺ lasing, but none of them have considered the competition between spontaneous emission and gain-swept lasing from N₂⁺ in the filamentation process. In this work, we experimentally investigate such competition by measuring the dynamic fluorescence distribution along the filament in the presence of an external probe pulse. The results show that the occurrence of lasing in the middle of the filament reduces the side fluorescence and the absorption of lasing in the rear part of the filament increases the fluorescence. By solving a time-dependent nonlinear Schrödinger equation and applying the transient ionization injection model, population distributions along the filament are numerically simulated and well explain our experimental observations.

I. INTRODUCTION

Femtosecond laser filamentation in the transparent medium is an interesting optical phenomenon as a result of the dynamic equilibrium between the Kerr self-focusing and the defocusing in the laser-induced plasma when an ultrashort laser pulse propagates nonlinearly through a transparent medium, allowing high laser intensity to be transferred over distances far beyond the Rayleigh length of the laser beam [1,2]. Its occurrence is normally accompanied by a variety of nonlinear effects such as white-light generation, third-order harmonic, pulse compression, pulse splitting, laserlike emission generation (or lasing) [3,4], etc. Among them, the lasing effect through the filament in gaseous media has received lots of attention in the past decade due to its potential applications for atmospheric remote sensing [5]. Two kinds of lasing effect in femtosecond filament were routinely investigated, i.e., lasing from neutral nitrogen molecules (N₂) [3,6,7] and single-ionized nitrogen molecules (N₂⁺) [4,8]. The physical mechanism of the former lasing has been well accepted as the electron-molecule inelastic collisions, in which the free electrons with enough kinetic energy are produced by circularly polarized laser pulses during filamentation [9]. On the contrary, the gain mechanism of N₂⁺ lasing has not been fully understood after almost ten years and has become a hot topic in the field of ultrafast optics.

N₂⁺ lasing occurs at 391- and 428-nm wavelengths, which are assigned to transitions $B\,^2\Sigma_u^+(v=0)\rightarrow X\,^2\Sigma_g^+(v'=0,1)$.

For convenience, $B\,^2\Sigma_u^+$, $A\,^2\Pi_u$, and $X\,^2\Sigma_g^+$ are termed as B, A, and X in the following context, respectively. The first observation of N₂⁺ lasing was reported by Yao *et al.*, in which the authors employed tunable mid-infrared femtosecond laser pulses to create filaments in air and observed strong laserlike emission at multiple wavelengths including 391 and 428 nm [4]. Soon after, Liu *et al.* as well as another two groups simultaneously observed strong N₂⁺ lasing by employing a single 800-nm femtosecond laser pulse to experience filament in pure nitrogen and air [8,10]. So far, various approaches such as the pump-probe technique [11], laser polarization modulation [12], few-cycle femtosecond laser [13], and mid-infrared lasers [14] have been applied to investigate the spatiotemporal characteristics, quantum coherence, optical gain dynamics, gain mechanisms, etc. On the one hand, some attempts like Raman scattering [15,16] and ultraviolet supercontinuum generation [17] with application of the N₂⁺ lasing as a remote detector have been carried out. On the other hand, several mechanisms have been proposed to explain the gain-buildup process of the N₂⁺ lasing, such as population inversion via transient ionization and coherent coupling [12,13,18–22], population inversion via electron recollision [23,24], and lasing without population inversion [25–27]. However, the electron recollision theory was later proved not to be the dominant mechanism [28,29]. Thereafter, there remains a very controversial issue for N₂⁺ lasing with and without inversion. On the one hand, the intermediate $A\,^2\Pi_u$ (termed as A) state is included, and population inversion between B and X state is established via A-X-B three-state coupling after ionization where the 800-nm pump laser resonantly promotes N₂⁺ from the X state to the B state. On the other hand, the quantum coherence of the different degrees of freedom established by

*These authors contributed equally to this work.
†dingpj@lzu.edu.cn
‡zyl@lzu.edu.cn

the femtosecond laser in the N_2^+ system also induces lasing even without population inversion, including electronic [14], vibrational [19,26,30], and rotational [27,31] coherence.

In the theoretical treatment of the N_2^+ lasing, space isotropic spontaneous radiation of N_2^+ at lasing wavelength was absolutely not considered in various models. However, as the lasing occurs in the longitudinal direction, it depletes the population of the upper B state and thus decreases the intensity of the spontaneous emission. Such competition would inevitably affect the final outcome of lasing intensity and its dependence on experimental parameters. In this work, we report on the evidence of dynamic competition between spontaneous emission and gain-swept lasing along the filament. Experimentally, the side fluorescence along the filament in the presence of lasing for various gas pressures and cases with or without a resonant probe pulse is investigated. Numerical simulated population distributions along the filament based on the transient ionization injection model qualitatively agree with our experimental observations.

II. EXPERIMENTAL SETUP

Experimentally, a 35-fs, 800-nm near-infrared laser pulse at 1-kHz repetition rate is emitted by a commercial Ti:sapphire laser system (Astrella, Coherent, Inc.). The laser pulse is split into two parts to build a pump-probe beam path. The linearly polarized pump laser beam with a pulse energy of ∼2.5 mJ is focused into a gas chamber filled with pure nitrogen by a 40-cm focal length lens to generate an approximately 2-cm-long filament. Another laser beam is frequency-doubled by a 200-μm thick β-barium borate crystal and used as a probe, whose pulse energy can be adjusted from 3 to 15 μJ by a combination of a half-wave plate and a polarizer. The center wavelength of the probe pulse is ∼395 nm. On the side of the gas chamber, a 6-cm focal length biconvex lens is used to image the filament. The imaging lens is placed about 12 cm away from the filament, and an inverted image reduced by a factor of 0.87 is generated about 23 cm away from the filament. Then the fluorescence spectrum is collected by measuring this image with a fiber with a 400-μm core diameter. By longitudinally moving the fiber head along the image, the fluorescence in different positions of the filament can be recorded. The forward absorption spectrum of the probe pulse and the side fluorescence spectrum are measured by a high-resolution spectrometer (Model 2061, McPherson, Inc.) with a 2400-lines/mm grating.

III. EXPERIMENTAL RESULTS AND DISCUSSIONS

To characterize the amplification of the probe pulse via the N_2^+ lasing, we denote the initial intensity of the probe pulse as I_0^p and that after passing through the filament as I^p. Both of these intensities are calculated by integrating the measured spectrum. Then, the optical density (OD) of the probe pulse is investigated. $\text{OD} = -\log_{10}(I^p/I_0^p)$ represents the absorption degree of the probe pulse through the whole filament and negative OD means amplification. In Fig. 1, the OD of the probe pulse is plotted as a function of the nitrogen pressure with different probe-pulse energies, where the time delay between
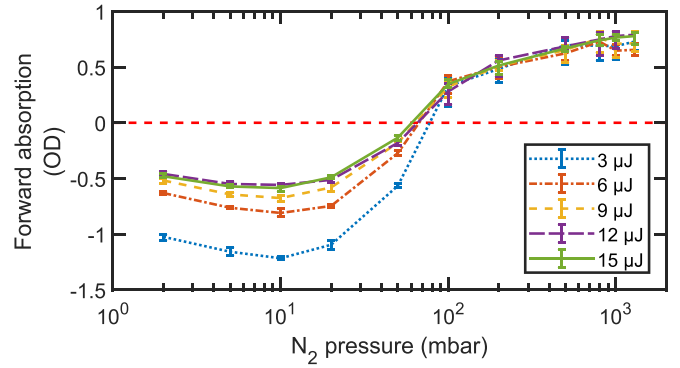

FIG. 1. The forward absorption of the probe pulse as a function of the gas pressure with different probe-pulse energies of 3 (blue dotted line), 6 (orange dash-dotted line), 9 (yellow short-dashed line), 12 (purple long-dashed line), and 15 (green solid line) μJ. The horizontal red dashed line is used to mark the zero OD.

two pulses is set to be ∼1 ps. We can see that the probe pulse is amplified at pressures less than ∼70 mbar due to the presence of optical gain in N_2^+ and is absorbed at pressures exceeding 70 mbar. On the other hand, as the probe energy increases from 3 to 15 μJ, the amplification of the probe pulse at low pressures (< 70 mbar) becomes weaker, while the absorption at high pressures (> 70 mbar) remains unchanged. It can be explained by a simple propagation model: $I^p = I_0^p e^{\alpha l}$, where α represents the gain (positive) or absorption (negative), and l is the propagation length. Here, α is determined by the status of the filament and it is obvious that α is proportional to OD but with opposite sign. When the incident intensity I_0^p is weak enough, the α is independent of I_0^p, such as the absorption in high-pressure cases. However, if the incident intensity I_0^p is too strong to be amplified or absorbed adequately, the output intensity I^p would approach I_0^p when I_0^p increased. In other words, α and the OD would approach zero, which is the same as the cases at low pressures. Thus, the amplification of the probe pulse is almost saturated with the energies we chose here but is not for absorption.

At the same time, the intensity of the fluorescence around 391 nm is measured as well. In Fig. 2(a), the longitudinal profiles of the fluorescence along the filament for various gas pressures are shown, in which the filament is generated by the pump pulse independently and starts from left to right. The zero position of the filament is defined by the geometrical focus of the lens. When the nitrogen pressure increases, the position of the strongest fluorescence intensity moves backward, which can be well understood by the self-focusing mechanism. The higher the pressure, the bigger the nonlinear Kerr index, and thus the intense laser has a shorter collapse length.

To investigate the relationship between the fluorescence and the gain-swept N_2^+ lasing, the longitudinal distribution of the side fluorescence from the filament along the propagation direction was measured with the presence of the external probe pulse. We denote the fluorescence intensities without and with the probe pulse as $I_{\text{w/o}}^f$ and $I_{\text{w/}}^f$, respectively. Figure 2(b) shows the relative fluorescence intensity $\gamma = \log_{10}(I_{\text{w/o}}^f/I_{\text{w/}}^f)$ as a function of the collecting positions of the filament for a large pressure range from 5 to 1000 mbar,
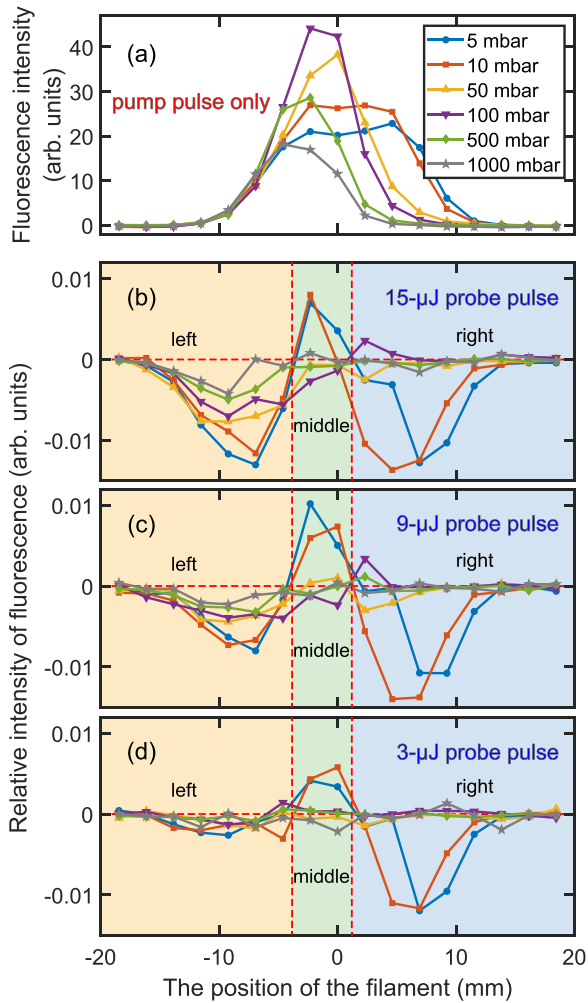
FIG. 2. (a) The longitudinal distribution of the side 391-nm fluorescence along the filament for gas pressure ranging from 5 to 1000 mbar when only the pump pulse exists. (b)–(d) The relative intensity γ of the 391-nm fluorescence from different positions of the filament for gas pressure ranging from 5 to 1000 mbar. The filament is generated from left to right. The energy of the probe pulse in panels (b) to (d) is set to 15, 9, and 3 μJ, respectively. The results at 5, 10, 50, 100, 500, and 1000 mbar are presented as blue circles, orange squares, yellow upward-pointing triangles, purple downward-pointing triangles, green diamonds, and gray pentagrams, respectively.

where the probe-pulse energy is set to 15 μJ. Naturally, $\gamma > 0$ suggests the side fluorescence is suppressed owing to the presence of the probe pulse, whereas $\gamma < 0$ means the opposite. At low pressures (< 50 mbar), the entire filament can be separated into three distinct regions. When the probe pulse propagates through the filament, the fluorescence intensity increases in the left and right regions, while decreasing in the middle region. When the pressure exceeds ~50 mbar, the fluorescence intensity changes induced by the probe pulse in the right and middle regions disappear, and the fluorescence enhancement in the left region reduces with the increasing pressure. The above results in Figs. 1 and 2(b) reveal the competition between the forward-lasing emission and the side fluorescence. At low pressures, the fluorescence intensity in

the middle region is suppressed because the probe pulse sweeps away a portion of the N_2^+ population in the upper $B(v = 0)$ state. At high pressures, absorption in the left of the filament dominates, and one can only observe the increase of the fluorescence intensity.

The competition between the side fluorescence and the forward lasing can be simply explained by their generation mechanisms. The 391-nm fluorescence is induced by the spontaneous emission whose intensity is proportional to the population of the $B(v = 0)$ state. While the 391-nm lasing is a kind of superradiance, its intensity is proportional to the population inversion between the $B(v = 0)$ and $X(v' = 0)$ states. Once the population inversion is established, the probe pulse will trigger the superradiance, which depletes a portion of the $B(v = 0)$ population and thus reduces the fluorescence intensity. On the other hand, if the population inversion does not exist, the probe pulse will be absorbed by the N_2^+ ion in the $X(v' = 0)$ state, which increases the $B(v = 0)$ population and thus the fluorescence intensity. The results suggest that the lasing emission can only be generated when the laser intensity is high enough, e.g., in the middle region of the filament at low pressures.

In the low-pressure case, one can also notice that the fluorescence intensity increases in the left and right regions with the presence of the probe pulse in Fig. 2(b), which means that there is absorption in these regions. To have a deeper learning about this absorption, the dependence of γ and probe-pulse energy is investigated. The longitudinal γ values with lower probe-pulse energies of 9 and 3 μJ are shown in Figs. 2(c) and 2(d), respectively. The most significant difference among Figs. 2(b)–2(d) is in the left region, where the absolute values of γ are decreased obviously when the weaker probe pulses are applied and become almost zero with a 3-μJ probe pulse. It is easy to understand that the higher the probe-pulse energy is the more population in the $X(v' = 0)$ state will be pumped to the excited $B(v = 0)$ state, which leads to stronger fluorescence intensity. As a result, the intenser the probe pulse, the stronger the absorption. This also agrees with the unsaturated absorption in Fig. 1. However, the fluorescence intensity in the middle and right regions is hardly influenced by the probe-pulse energy. As γ remains almost zero at high pressures ($\geqslant 50$ mbar), we only discuss the results at lower pressures in these two regions. As we discussed in Fig. 1, the probe-pulse energy (in the magnitude of μJ) in this work is much stronger than that used in previous works (in the magnitude of nJ) so that the amplification of the probe pulse is close to saturated. Thus, the values of γ in the middle region slightly become larger when the probe energy increases from 3 to 9 μJ, but are relatively unchanged when the probe energy increases to 15 μJ in Figs. 2(b)–2(d). On the other hand, the negative γ in the right region represents the existence of absorption. Unlike the left region, its insensitivity to the probe-pulse energy means that this absorption is not for the probe pulse but for the forward-lasing emission generated in the middle region.

Additionally, the spectra of the forward lasing at different pressures are measured in Figs. 3(c)–3(h). The side fluorescence spectrum of the $B(v = 0) \rightarrow X(v' = 0)$ transition at 100 mbar in Figs. 3(a) and 3(b) is used as the calibration of rotational lines of the forward lasing. The self-seeded (only pump pulse) and external-seeded (the probe pulse acts as
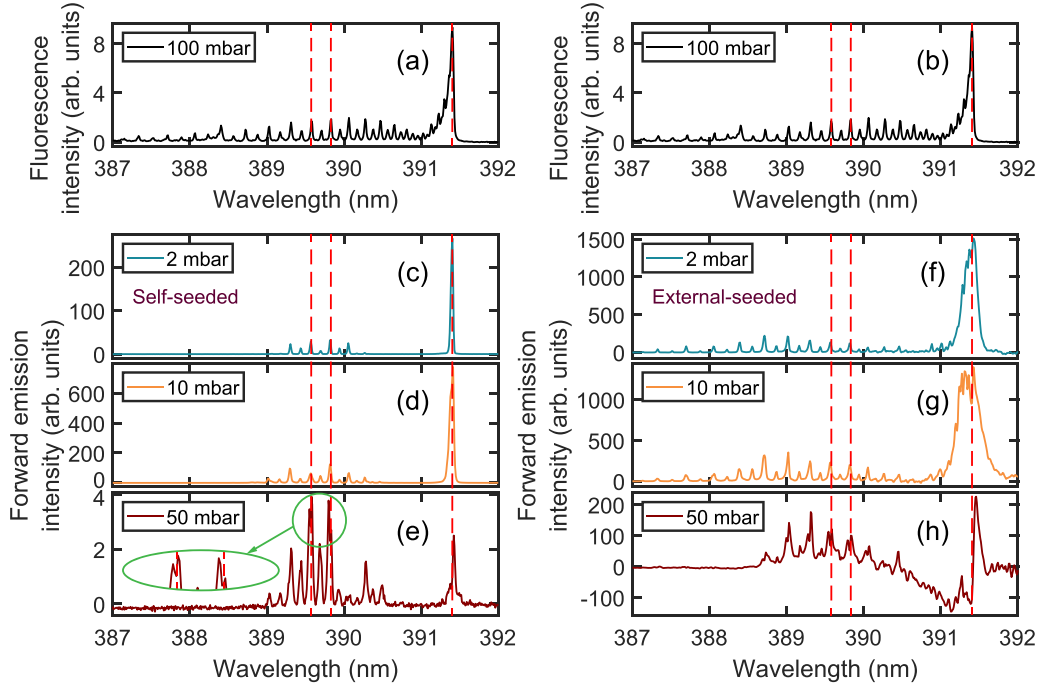
FIG. 3. (a) and (b) The side fluorescence spectrum of the transition $B\,^2\Sigma_u^+(v=0) \to X\,^2\Sigma_g^+(v'=0)$ at 100 mbar. (c)–(e) The self-seeded forward-lasing spectra at 2, 10, and 50 mbar, respectively. (f)–(h) The forward-lasing spectra externally seeded by a 15-μJ probe pulse at 2, 10, and 50 mbar, respectively.

a seed pulse) forward-lasing spectra at different pressures are shown in the left column [Figs. 3(c)–3(e)] and the right column [Figs. 3(f)–3(h)], respectively. In self-seeded cases, the position of the *P* branch bandhead deviates from that in the fluorescence spectrum, and two rotational lines in the *R* branch are split at 50 mbar, which is shown zoomed-in in Fig. 3(e). When the probe pulse acts as the external seed, the *P* branch of the forward lasing is significantly broadened, and the peak splitting is more obvious, especially in the *P* branch. The spectrum broadening is induced by the appearance and superposition of rotational lines in the *P* branch, which can be compared by the separate lines in the *R* branch. Besides, the spectral splitting based on the propagation effect has also been reported recently [32]. By comparing Fig. 2(b) and Figs. 3(f)-3(h), it is obvious that fluorescence increment in the right filament is related to the strong forward air lasing at 5 and 10 mbar. It suggests that the absorption of the forward-lasing emission in the right filament is an indispensable repercussion for the lasing emission. It might be efficient to improve the lasing intensity by shorting or cutting off the right region of the filament. Besides, it should also be noticed that the lasing intensity at 50 mbar is only about 2% of that at 10 mbar, which is too weak to affect the side fluorescence intensity in Fig. 2.

To understand the competition better, the laser intensity and the population distribution in the filament are simulated. We first employ a TDNSE to simulate the pump-pulse propagation process as in Eq. (1), which could also be called the nonlinear envelope equation:

$$\partial_z U = \frac{i}{2k_0}T^{-1}\nabla_\perp U + iDU + i\frac{\omega_0}{c}n_2 T|U|^2$$
$$-i\frac{k_0}{2n_0\rho_c}T^{-1}\rho U - \frac{\beta^{(\kappa)}}{2}|U|^{2\kappa-2}U - \frac{\sigma}{2}\rho U. \quad (1)$$

It describes a forward-propagating pulse going through different linear and nonlinear effects, such as diffraction, dispersion, optical Kerr effect, and plasma effect during laser-matter interaction. Its effectiveness has been proved in both gas and solid medium [33–36]. Here, $U(r,z,t)|_{z=0} = e^{-r^2/R^2 - t^2/\tau^2}F_{\text{lens}}$ is the electric-field envelope, and $F_{\text{lens}} = e^{-ik_0 r_0^2/2f}$ represents the phase change by the focusing lens of the input beam, where k_0, r_0, and f are the wave vector of pulses, the beam radius, and the focal length, respectively. In the first term of the formula, $T = 1 + (i/\omega_0)(\partial/\partial t)$ and $\nabla_\perp$ are the spatiotemporal coupling operator and the spatial second-order differential operator, respectively [37]. Then D is the dispersion coefficients at the center frequency which includes group-velocity dispersion and third-order dispersion, ω_0 is the central angular frequency, and the nonlinear refractive index n_2 is dependent on the variation of the N_2 pressure [38]. Moreover, the following terms are responding to plasma-related processes, which are related to the plasma density ρ directly, where n_0, ρ_c, $\beta^{(\kappa)}$, κ, and σ donate the linear refractive index, the critical plasma density of the medium, the coefficient for multiphoton absorption, the ionization order, and the cross section of collisional ionization, respectively. We apply the MO-ADK model for the photoionization rates in our circumstance; details of these parameters have been discussed previously [39].

In the simulation, a 2.5-mJ pump pulse is focused in 5-, 50-, and 500-mbar pure nitrogen gas by a 400-mm planoconvex lens. Figure 4(a) is the simulated laser intensity in the filament region, and the position of 0 mm is the geometrical focus of the lens. The laser intensity has a wide range from 10^{13} to 10^{14} W/cm^2 along the filament. The strongest intensity position is close to the geometrical focus as expected, and this position moves backward with the increasing
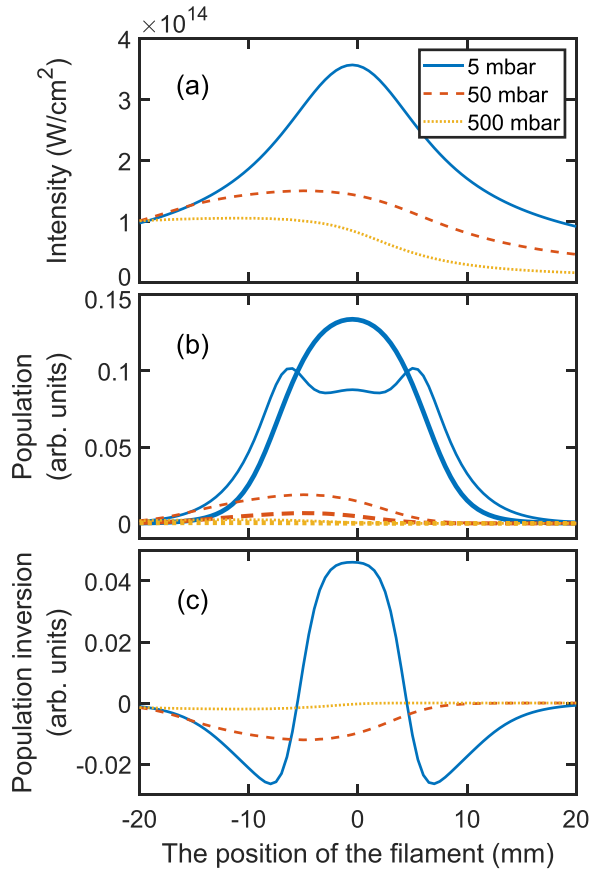
FIG. 4. The simulated laser intensity distribution (a), the population distribution of $B\,^2\Sigma_u^+(v=0)$ (thick lines) and $X\,^2\Sigma_g^+(v'=0)$ (thin lines) states (b), and the population inversion (c) along the filament at 5 (blue solid lines), 50 (orange dashed lines), and 500 (yellow dotted lines) mbar.

pressure, which is because of the stronger self-focusing at higher pressures. Meanwhile, the stronger intensity clamping at high pressures leads to the lower intensity.

Based on the simulated laser intensity, we further calculate the population distribution of $X(v'=0)$ and $B(v=0)$ states of the N_2^+ by applying the transient ionization injection model [20], as shown with solid and dashed lines, respectively, in Fig. 4(b). At high pressures (50 and 500 mbar), the simulations show that the population injection to the N_2^+ ion states occurs considerably when the laser intensity $\gtrsim 1 \times 10^{14}$ W/cm^2. The more intense the laser, the greater the populations of two states, and the population of the $X(v'=0)$ state is always larger than that of the $B(v=0)$ state. However, the proportional relation between the $X(v=0)$ state

population and the intensity is interrupted due to the coherent coupling between A and X states when the laser intensity is higher than $\sim 2.5 \times 10^{14}$ W/cm^2 at 5 mbar. As a result, the population inversion is established in the middle of the filament at this pressure with high laser intensity ($\gtrsim 2.8 \times 10^{14}$ W/cm^2), but not at both edges of the filament at 5 mbar and in the whole filament at high pressures (50 and 500 mbar), which is manifested as the population inversion in Fig. 4(c). Therefore, the experimental results in Fig. 3(b) can be well explained by the population inversion between $X(v'=0)$ and $B(v=0)$ states. At low pressures (< 50 mbar), the fluorescence intensity decrease in the middle region is induced by the population depletion of the $B(v=0)$ state when the probe pulse triggers the population-inversion-based superradiance. In the left and right regions, the population inversion is not established, and the population of the $B(v=0)$ state becomes larger by absorbing the probe pulse and the forward-lasing emission, respectively. Thus, the fluorescence intensity increases in these two regions. As for higher pressures, there is no population inversion in the whole filament, and only the absorption to the probe pulse exists.

IV. CONCLUSION

In conclusion, we observed the competition between the forward superradiance and the side fluorescence from N_2^+ during the filamentation of a strong 800-nm femtosecond laser pulse in low-pressure nitrogen gas by measuring the longitudinal distribution of the side fluorescence under the influence of a resonant probe pulse with different gas pressures. It was observed that the N_2^+ lasing occurs in the middle of the filament at the expense of the fluorescence, whereas the fluorescence is enhanced on two sides of the filament. Numerical simulations of population distributions of the N_2^+ well explain the above experimental observations. Our results suggest that the physical models of the N_2^+ lasing should include the competition effect between spontaneous emission and gain-swept lasing emission in order to more precisely predict the behavior of the N_2^+ lasing.

[1] J. Kasparian, M. Rodriguez, G. Méjean, J. Yu, E. Salmon, H. Wille, R. Bourayou, S. Frey, Y.-B. André, A. Mysyrowicz, R. Sauerbrey, J.-P. Wolf, and L. Wöste, White-light filaments for atmospheric analysis, Science **301**, 61 (2003).

[2] A. Couairon and A. Mysyrowicz, Femtosecond filamentation in transparent media, Phys. Rep. **441**, 47 (2007).

[3] Q. Luo, W. Liu, and S. Chin, Lasing action in air induced by ultra-fast laser filamentation, Appl. Phys. B **76**, 337 (2003).

[4] J. Yao, B. Zeng, H. Xu, G. Li, W. Chu, J. Ni, H. Zhang, S. L. Chin, Y. Cheng, and Z. Xu, High-brightness switchable multiwavelength remote laser in air, Phys. Rev. A **84**, 051802(R) (2011).

[5] Y. C. Pavel Polynkin, *Air Lasing*, 1st ed. (Springer, Cham, 2018).

[6] S. Mitryukovskiy, Y. Liu, P. Ding, A. Houard, and A. Mysyrowicz, Backward stimulated radiation from filaments in nitrogen gas and air pumped by circularly polarized 800 nm femtosecond laser pulses, Opt. Express **22**, 12750 (2014).

[7] P. Ding, S. Mitryukovskiy, A. Houard, E. Oliva, A. Couairon, A. Mysyrowicz, and Y. Liu, Backward lasing of air plasma pumped by circularly polarized femtosecond pulses for the sake of remote sensing (BLACK), Opt. Express **22**, 29964 (2014).

[8] Y. Liu, Y. Brelet, G. Point, A. Houard, and A. Mysyrowicz, Self-seeded lasing in ionized air pumped by 800 nm femtosecond laser pulses, Opt. Express **21**, 22791 (2013).

[9] S. Mitryukovskiy, Y. Liu, P. Ding, A. Houard, A. Couairon, and A. Mysyrowicz, Plasma luminescence from femtosecond filaments in air: Evidence for impact excitation with circularly polarized light pulses, Phys. Rev. Lett. **114**, 063003 (2015).

[10] T.-J. Wang, J.-F. Daigle, J. Ju, S. Yuan, R. Li, and S. L. Chin, Forward lasing action at multiple wavelengths seeded by white light from a femtosecond laser filament in air, Phys. Rev. A **88**, 053429 (2013).

[11] J. Yao, G. Li, C. Jing, B. Zeng, W. Chu, J. Ni, H. Zhang, H. Xie, C. Zhang, H. Li, H. Xu, S. L. Chin, Y. Cheng, and Z. Xu, Remote creation of coherent emissions in air with two-color ultrafast laser pulses, New J. Phys. **15**, 023046 (2013).

[12] H. Li, M. Hou, H. Zang, Y. Fu, E. Lötstedt, T. Ando, A. Iwasaki, K. Yamanouchi, and H. Xu, Significant enhancement of N_2^+ lasing by polarization-modulated ultrashort laser pulses, Phys. Rev. Lett. **122**, 013202 (2019).

[13] H. Xu, E. Lötstedt, A. Iwasaki, and K. Yamanouchi, Sub-10-fs population inversion in N_2^+ in air lasing through multiple state coupling, Nat. Commun. **6**, 8347 (2015).

[14] J. Chen, J. Yao, H. Zhang, Z. Liu, B. Xu, W. Chu, L. Qiao, Z. Wang, J. Fatome, O. Faucher, C. Wu, and Y. Cheng, Electronic-coherence-mediated molecular nitrogen-ion lasing in a strong laser field, Phys. Rev. A **100**, 031402(R) (2019).

[15] X. Zhao, S. Nolte, and R. Ackermann, Lasing of N_2^+ induced by filamentation in air as a probe for femtosecond coherent anti-Stokes raman scattering, Opt. Lett. **45**, 3661 (2020).

[16] Z. Zhang, F. Zhang, B. Xu, H. Xie, B. Fu, X. Lu, N. Zhang, S. Yu, J. Yao, Y. Cheng, and Z. Xu, High-sensitivity gas detection with air-lasing-assisted coherent Raman spectroscopy, Ultrafast Sci. **2022**, 9761458 (2022).

[17] H. Lei, J. Yao, J. Zhao, H. Xie, F. Zhang, H. Zhang, N. Zhang, G. Li, Q. Zhang, X. Wang, Y. Yang, L. Yuan, Y. Cheng, and Z. Zhao, Ultraviolet supercontinuum generation driven by ionic coherence in a strong laser field, Nat. Commun. **13**, 4080 (2022).

[18] J. Yao, S. Jiang, W. Chu, B. Zeng, C. Wu, R. Lu, Z. Li, H. Xie, G. Li, C. Yu, Z. Wang, H. Jiang, Q. Gong, and Y. Cheng, Population redistribution among multiple electronic states of molecular nitrogen ions in strong laser fields, Phys. Rev. Lett. **116**, 143007 (2016).

[19] T. Ando, E. Lötstedt, A. Iwasaki, H. Li, Y. Fu, S. Wang, H. Xu, and K. Yamanouchi, Rotational, vibrational, and electronic modulations in N_2^+ lasing at 391 nm: Evidence of coherent $B^2\Sigma_u^+ - X^2\Sigma_g^+ - A^2\Pi_u$ coupling, Phys. Rev. Lett. **123**, 203201 (2019).

[20] Q. Zhang, H. Xie, G. Li, X. Wang, H. Lei, J. Zhao, Z. Chen, J. Yao, Y. Cheng, and Z. Zhao, Sub-cycle coherent control of ionic dynamics via transient ionization injection, Commun. Phys. **3**, 50 (2020).

[21] H. Lei, G. Li, H. Xie, Q. Zhang, X. Wang, J. Zhao, Z. Chen, and Z. Zhao, Mechanism and control of rotational coherence in femtosecond laser-driven N_2^+, Opt. Express **28**, 22829 (2020).

[22] X. Hongqiang, L. Hongbin, G. Li, J. Yao, Z. Qian, X. Wang, J. Zhao, Z. Chen, H. Sun, and Z. Zhao, Controlling the collective radiative decay of molecularions in strong laser fields, Photonics Res. **9**, 2046 (2021).

[23] Y. Liu, P. Ding, G. Lambert, A. Houard, V. Tikhonchuk, and A. Mysyrowicz, Recollision-induced superradiance of ionized nitrogen molecules, Phys. Rev. Lett. **115**, 133203 (2015).

[24] Y. Liu, P. Ding, N. Ibrakovic, S. Bengtsson, S. Chen, R. Danylo, E. R. Simpson, E. W. Larsen, X. Zhang, Z. Fan, A. Houard, J. Mauritsson, A. L'Huillier, C. L. Arnold, S. Zhuang, V. Tikhonchuk, and A. Mysyrowicz, Unexpected sensitivity of nitrogen ions superradiant emission on pump laser wavelength and duration, Phys. Rev. Lett. **119**, 203205 (2017).

[25] L. Arissian, B. Kamer, A. Rastegari, D. M. Villeneuve, and J.-C. Diels, Transient gain from N_2^+ in light filaments, Phys. Rev. A **98**, 053438 (2018).

[26] A. Mysyrowicz, R. Danylo, A. Houard, V. Tikhonchuk, X. Zhang, Z. Fan, Q. Liang, S. Zhuang, L. Yuan, and Y. Liu, Lasing without population inversion in N_2^+, APL Photonics **4**, 110807 (2019).

[27] M. Richter, M. Lytova, F. Morales, S. Haessler, O. Smirnova, M. Spanner, and M. Ivanov, Rotational quantum beat lasing without inversion, Optica **7**, 586 (2020).

[28] M. Britton, P. Laferrière, D. H. Ko, Z. Li, F. Kong, G. Brown, A. Naumov, C. Zhang, L. Arissian, and P. B. Corkum, Testing the role of recollision in N_2^+ air lasing, Phys. Rev. Lett. **120**, 133208 (2018).

[29] H. Li, Q. Song, J. Yao, Z. Liu, J. Chen, B. Xu, K. Lin, J. Qiang, B. He, H. Xu, Y. Cheng, H. Zeng, and J. Wu, Air lasing from singly ionized N_2 driven by bicircular two-color fields, Phys. Rev. A **99**, 053413 (2019).

[30] X. Zhang, Q. Lu, Z. Zhang, Z. Fan, D. Zhou, Q. Liang, L. Yuan, S. Zhuang, K. Dorfman, and Y. Liu, Coherent control of the multiple wavelength lasing of N_2^+: Coherence transfer and beyond, Optica **8**, 668 (2021).

[31] H. Xie, H. Lei, G. Li, Q. Zhang, X. Wang, J. Zhao, Z. Chen, J. Yao, Y. Cheng, and Z. Zhao, Role of rotational coherence in femtosecond-pulse-driven nitrogen ion lasing, Phys. Rev. Res. **2**, 023329 (2020).

[32] Q. Lu, X. Zhang, S. López, H. Mei, L. Xu, Q. Liang, A. Houard, V. Tikhonchuk, A. Mysyrowicz, E. Oliva, and Y. Liu, Spectral splitting of the lasing emission of nitrogen ions pumped by 800-nm femtosecond laser pulses, Opt. Lett. **48**, 664 (2023).

[33] N. L. Wagner, E. A. Gibson, T. Popmintchev, I. P. Christov, M. M. Murnane, and H. C. Kapteyn, Self-compression of ultrashort pulses through ionization-induced spatiotemporal reshaping, Phys. Rev. Lett. **93**, 173902 (2004).

[34] Y.-C. Cheng, C.-H. Lu, Y.-Y. Lin, and A. H. Kung, Supercontinuum generation in a multi-plate medium, Opt. Express **24**, 7224 (2016).

[35] Y. Gao, Y. Su, S. Xu, X. Zhu, K. Zhao, S. Fang, J. Zhu, and Z. Wei, Generation of annular femtosecond few-cycle pulses by self-compression and spatial filtering in solid thin plates, Opt. Express **29**, 29789 (2021).

[36] Y. Gao, X. Wang, X. Zhu, K. Zhao, H. Liu, Z. Wang, S. Fang, and Z. Wei, Quantification and analysis of the nonlinear effects in spectral broadening through solid medium of femtosecond pulses by neural network, Phys. Rev. Res. **4**, 013035 (2022).

[37] L. Bergé, S. Skupin, R. Nuter, J. Kasparian, and J.-P. Wolf, Ultrashort filaments of light in weakly ionized, optically transparent media, Rep. Prog. Phys. **70**, 1633 (2007).

[38] A. Börzsönyi, Z. Heiner, A. Kovács, M. P. Kalashnikov, and K. Osvay, Measurement of pressure dependent nonlinear refractive index of inert gases, Opt. Express **18**, 25847 (2010).

[39] X. M. Tong, Z. X. Zhao, and C. D. Lin, Theory of molecular tunneling ionization, Phys. Rev. A **66**, 033402 (2002).